Simulation and optimization of a miniaturized ion source for a neutron tube

Ailin Zhang,[1] Dong Li,[2] Lechen Xu,[1] Zijian Xiong,[1]
Junyi Zhang,[1] Haiping Peng,[1] and Qing Luo[1,*]

[1]*State Key Laboratory of Particle Detection and Electronics, National Synchrotron Radiation Laboratory, Department of Modern Physics, University of Science and Technology of China, Hefei 230026, People's Republic of China*

[2]*Geological Environment Monitoring Station of Wanzhou, Chongqing 404000, People's Republic of China*

(Received 26 May 2022; accepted 26 September 2022; published 17 October 2022)

A miniaturized Penning ion source, capable of generating a milliampere H^+ beam with low anode power supply and low gas consumption, was produced and tested for neutron tubes. For a better understanding and optimization of the Penning ion source, magnetic field, beam extraction system, and plasma simulations were conducted to research the optimization of the Penning ion source. The distance between the two cathodes is optimized based on the plasma simulations. Based on the optimization of the magnetic field, extraction system, and the distance of the cathodes, the extraction current of the Penning source had been increased from 1.21 to 1.72 mA, and the H^+ ratio had been increased from 36% to 42.3%.

DOI: 10.1103/PhysRevAccelBeams.25.103501

I. INTRODUCTION

Penning ion sources enjoy a long history and mature technology. In 1937, Penning and Moubis discovered the Penning discharge; on this basis, Lorrain and Keller developed the first Penning proton source in 1947 [1]. Penning sources have the advantages of simple structure and convenient operation and are widely used in many compact devices such as small accelerators, detectors, ion implanters, and neutron tubes. [2–5]. Because of their small size, low-level work pressure, and high reliability, Penning ion sources are employed in sealed neutron tubes, which are widely used in oil logging, identifying fissile elements in cargo, coal quality investigation, and structural evaluation [6–8]. Although Penning ion sources have been utilized in a variety of applications and various sources have been investigated, many of the prior designs are sophisticated, expensive, or tailored for a specific application. Furthermore, many references [4–14] do not fully specify their source dimensions, manufacturing processes, or capabilities, making it difficult to build and use Penning ion sources in different applications. A simple, inexpensive Penning ion source that can be fabricated with basic machining skills and standard laboratory accessories is described and optimized with a plasma model in this paper. This allows for a large-scale rollout in neutron tube manufacturing.

The structure of the neutron tube is shown in Fig. 1, the ion source of the neutron tube produces 80-keV deuterium ions to bombard the tritium target, resulting in a fusion reaction that produces 14-MeV neutrons. The seal neutron tubes are mainly used for oil exploration wells in this paper. Oil wells are usually only a few hundred millimeters in diameter and several hundred meters in depth, so it is difficult to supply power and gas. The gas supply is obtained by heating the deuterium storage material as shown in Fig. 1. The Penning source before optimization can obtain a current intensity of 1.21 mA @80 kV, and the lifetime after sealing is about 145 h, under the anode power of 2 kV@1250 mA (2.5 kW) and the intake deuterium of 0.12 sccm. In order to increase the lifetime and application scenarios(application in deeper oil wells) of neutron tubes, it is required that the new Penning source generate a high current with the low power($<$1.5 kW) and low gas supply ($<$0.1 sccm), and the outer diameter of the ion source should be as small as possible, and the beam current no more than 2 mA (high voltage power supply $<$160 W), it is not realistic to provide a high voltage of 80 kV underground with a high current.

In the past 10 years, dozens of Penning sources have been manufactured through experimental optimization. Although the structure of the Penning source is simple, the optimizations in low power and low gas supply are very complicated and difficult. In order to optimize the Penning ion source more efficiently, a plasma model is established to simulate Penning discharge. The magnetic field configuration, extraction structure, and cathode spacing of the Penning source are simulated and optimized in this paper.

*Corresponding author.
Luoqing@ustc.edu.cn

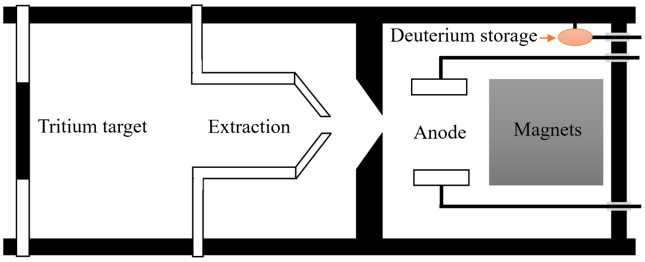

FIG. 1. The neutron tube structure diagram.

Optimization simulation research on gas pressure, anode voltage, and discharge chamber size is carried out. Through a plasma simulation, the best parameters are found, and finally, we manufacture the Penning source based on the optimized parameters, carry out experimental research, and compare the results with the plasma simulation results. A lot of experimental results show that the discharge of deuterium is better than that of hydrogen, so the neutron tubes are usually tested with hydrogen discharge before they are applied online. The Penning source will be transferred to a suitably qualified laboratory in the future to test the neutron yield.

II. MECHANICAL STRUCTURE OF THE PENNING ION SOURCE

The Penning ion source operates at low gas pressure and high voltage between two cathodes and an anode, which consists of two main components: an ion formation system and an axial ion extraction system. The ion formation consists of two opposite cathodes, a barrel-type anode, and a permanent magnet. The anode is a 6-mm diameter aluminum cylinder that has been machined to the dimensions and geometry shown in Fig. 2, aluminum will form a thin layer of aluminum oxide after being exposed to air which has a high secondary electron coefficient. The cathode is tungsten and the ceramic is made of alumina. A permanent magnet with a surface flux density of approximately 0.8 T is encased in a 0.5-mm-thick nonmagnetic stainless steel sleeve and pressed on the cathode. There is a circle of soft iron on the periphery of the anticathode for adjusting the magnetic field lines. By adjusting the size and material of the soft iron, the configuration of the magnetic field can be optimized. The Penning source is an experimental test source with a flexible design. The cathode, anticathode, and anode are all removable and replaceable. By adjusting the size of the two cathodes and anode, the distance between the two cathodes can be changed so that we can determine the optimal discharge gap. The current test source has an outer diameter of 33 mm. In the future, the optimized Penning source will be sealed by welding as a neutron tube, and the outer diameter of the mass-produced sealed neutron tube will be only 28 mm.

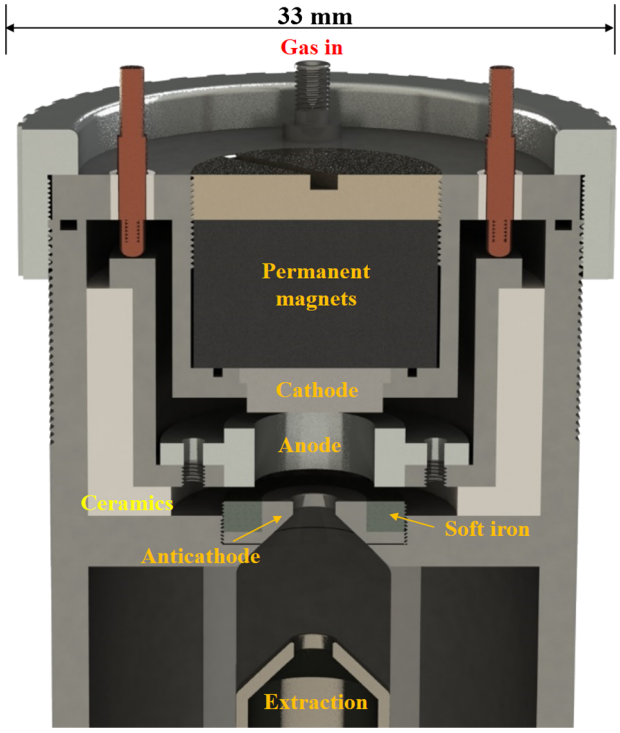

FIG. 2. Framework of the Penning source.

III. MAGNETIC FIELD OPTIMIZATION

In a typical Penning ion source, when ionization begins, the electrons move toward the anode under the action of an electric field; when a magnetic field is applied, the electrons spiral and do not hit the anode wall directly. Electrons will

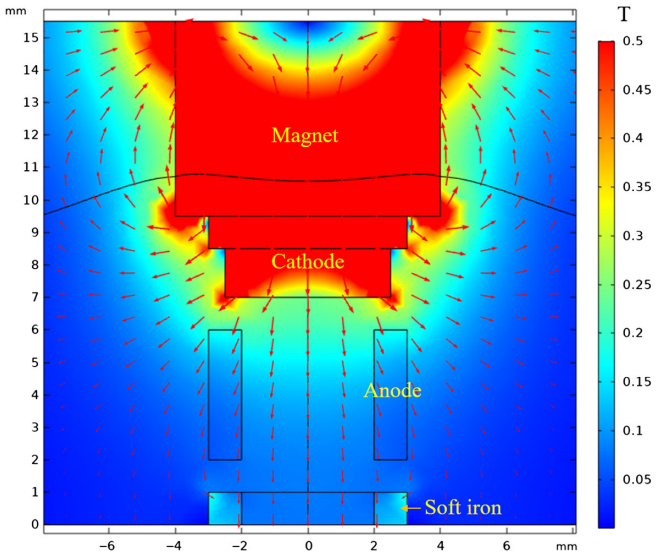

FIG. 3. The optimized magnetic field simulation result of the Penning ion source. Surface: magnetic flux density norm (T), contour: magnetic scalar potential (A), arrow surface: magnetic flux density.

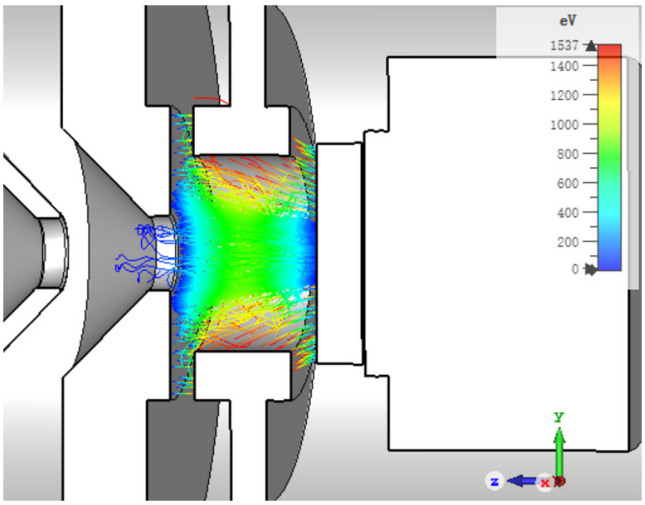

FIG. 4. The optimized magnetic field simulation result of the Penning ion source.

undergo Larmor rotation along the magnetic field lines, which can collide with more gas molecules for higher ionization efficiency, so the magnetic field is crucial for the Penning source. The magnetic field optimization of Penning source is a particularly time-consuming task requiring extensive experimental attempts, dozens of Penning sources were designed to test various magnetic fields, which are inefficient and expensive. In those experiments, it is found that the three magnetic rings can greatly improve the discharge efficiency of this Penning source, but this will cause the outer diameter of the source to be too large. To enhance the uniformity of the axial magnetic field of the ion source, soft iron was used in the Penning ion source, as shown in Fig. 3. The soft iron can be disassembled, and its shape, size, and material type can be changed. In order to optimize the magnetic field more efficiently, a plasma model was established to simulate various magnetic field configurations (more details in Chap. 5), obtained the best magnetic field configuration, and then verified it through experiments. The simulation and experimental results show that the magnetic field in the plasma region parallel to the anode is beneficial to the plasma density and stability. A soft iron with a relative magnetic permeability of approximately 400 is recommended to be installed on the periphery of the anticathode.

To further verify the reliability of the magnetic field, simulations of the electron tracks are performed with CST Studio Suite [15]. A dc voltage of 1.5 kV is applied to the anode, and the electrons undergo Larmor rotation under the action of the magnetic field and the electric field. The trajectory simulation results are shown in Fig. 4. It can be seen that the mean free path and lifetime of the electrons have been in a good state.

IV. EXTRACTION SYSTEM OPTIMIZATION

In order to reduce the size of the tritium target to reduce the cost of the neutron tube, the extraction system needs to be optimized to reduce the beam diameter on the tritium target. The original Penning source was two flat electrodes (2 mm diameter holes with a distance of 9 mm), the distance between the plasma emission surface and the tritium target was 38.5 mm, and the diameter of the beam on the target was 11 mm. The original extraction system still has a small spark problem, so the electrode spacing has been increased to 11 mm, the diameter of the extraction hole is still 2 mm, and the distance between the plasma emission surface and the tritium target has been increased

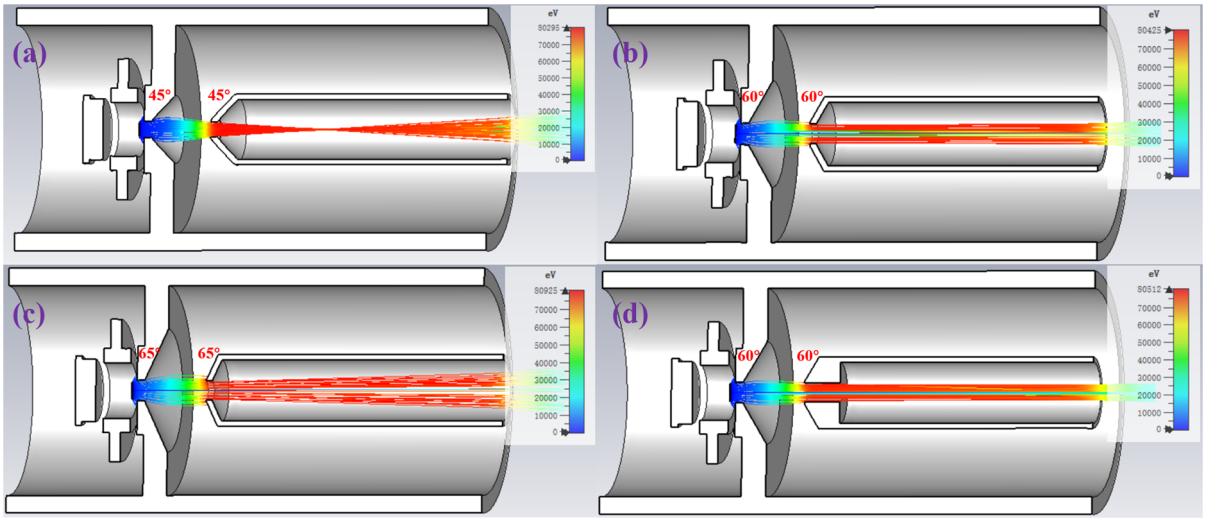

FIG. 5. Simulation results of deuterium ion extraction under different extraction electrode structures. The extraction voltage is fixed at −80 kV. (a) electrode angle of 45°, (b) electrode angle of 60°, (c) electrode angle of 65°, (d) electrode angle of 60° with collimation.

TABLE I. Comparison of simulation and experimental results of beam spot size at tritium targets with different electrodes (The currents are all experimental results).

Electrode type	Simulation beam size (mm)	Experiment beam size (mm)	Current (mA)
Flat electrodes	9.0	9.2	1.21
(a) type	3.4	3.7	1.76
(c) type	3.2	3.5	1.75
(d) type	2.4	2.7	1.71

to 41 mm. A series of electrode optimization simulation studies is carried out, as shown in Fig. 4. In the simulations, the plasma emission surface is assumed to be flat.

It is found by calculation that the angle and voltage of the electrode determine whether it focuses or diverges from the ion beam. To generate enough neutrons when the deuterium beam bombards the target, our extraction voltage is set at −80 kV. We perform beam extraction simulations for electrode angles of 40°, 45°, 50°, 55°, 60°, and 65°. It is found that electrodes with an angle of 60° and less than 65° have an overly strong focusing effect on the ion beam, which causes the beam to cross and rediverge, similar to the 45° electrode, as shown in Fig. 5(a). As the electrode angle increases, its focusing effect on the beam gradually weakens, and when it increases to 60°, the focusing force can just offset the space charge effect brought by the beam itself; the increase in the beam's diameter is reduced, as shown in Fig. 5(b). When continuing to increase the electrode angle to 65°, the focal length effect becomes too weak, and the beam becomes divergent, as shown in Fig. 5(c). In addition, we add collimation to the high-voltage electrode at the optimal angle of 60°, as shown in Fig. 5(d), which can make the beam radius smaller.

The extraction experimental studies had been carried out, but the fast emittance measurement unit [16,17] is not suitable here because of its small beam diameter, a radiochromic film (RCF) detector was used to measure the beam spot size, and the measurement results are shown in Table I. The experimental results for flat electrodes are the results before optimization. The experimental results for (a), (c), and (d) type electrodes are results after the source optimization. In the design of (d) type electrode, the collimation causes a beam loss of 0.04 mA. The (d) type electrode is the best choice which has a smaller bombardment point makes smaller the neutron emission source will be beneficial to tritium target manufacturing and the analysis of the detection signal.

V. PLASMA SIMULATION

Although the structure of the Penning source is very simple, there are still many parameters that can be optimized for its operation and structure, such as anode voltage, gas pressure, anode inner diameter, cathode spacing, cathode material, magnetic field configuration, etc., which are all crucial to the formation of plasma, therefore, a 3D fluid model [18,19] with an electromagnetic field sustained through anode power supply and permanent magnets is performed using COMSOL. The drift-diffusion equations are used to describe the transport of electron and the electron energy, as in Ref [20]. By solving a pair of drift diffusion equations for the electron density and the mean electron energy, the electron density and mean electron energy are computed. Electron convection due to fluid flow is ignored. For basic details on the transportation of electrons,

$$\frac{\partial}{\partial t}(n_e) + \nabla \cdot [-n_e(\boldsymbol{\mu_e} \cdot \mathbf{E}) - \mathbf{D}_e \cdot \nabla n_e] = S_e \quad (1)$$

$$\frac{\partial}{\partial t}(n_\varepsilon) + \nabla \cdot [-n_\varepsilon(\mu_\varepsilon \cdot \boldsymbol{E}) - \boldsymbol{D}_\varepsilon \cdot \nabla n_\varepsilon] + \boldsymbol{E} \cdot \Gamma_e = S_\varepsilon \quad (2)$$

where the electron source is given by $S_e = \sum_{j=1}^{M} x_j k_j N_n n_e$, x_j is the mole fraction of the target species for reaction j, k_j is the rate coefficient for reaction j, and N_n is the total neutral number density. The electron energy loss due to inelastic collisions is obtained by summing the collisional energy loss over all reactions, $S_\varepsilon = \sum_{j=1}^{P} x_j k_j N_n n_e \Delta\varepsilon_j$.

Combined with the electron energy distribution functions (EEDFs) [21], the r rate coefficients were obtained,

$$k = \gamma \int_0^\infty \varepsilon f(\varepsilon)\sigma(\varepsilon) d\varepsilon \quad (3)$$

where $\gamma = (2q/m_e)^{1/2}$, me is the electron mass, ε is energy, σk is the collision cross section, f is the electron energy distribution function, and $f(\varepsilon)$ is the non-Maxwellian EEDF, which can be calculated by solving the Boltzmann equation [22]. In this paper, the EEDF will be taken as the previous data [23], and $\sigma(\varepsilon)$ is the corresponding collision cross section.

Penning plasma is a nonequilibrium type of plasma, so electrons, ions, and neutrals have individual temperatures, typically expressed as electron temperature > ion temperature > neutral gas temperature. [23]. The neutral gas temperature is assumed to be 0.1 eV, and the ion temperature is assumed to be 0.5 eV. The major processes in the Penning plasma are thought to be these 12 reactions, as shown in Table II.

Figure 6 indicates the calculated volume reaction rate coefficients $\sigma(\varepsilon)$, where T represents the electron temperature and ion temperature for electron reactions and heavy particulate reactions, respectively. In addition, the rate coefficients of the heavy particle reactions are compared to the target particles.

TABLE II. List of the main processes of hydrogen plasma inside the positive ion source.

No.	Reactions	Description	Rate coefficients
1	$e + H_2 \rightarrow 2H + e$	Dissociation	α_1
2	$H + H + \text{wall} \rightarrow H_2 + \text{wall}$	H wall recombination	α_2
3	$e + H \rightarrow H^+ + 2e$	H ionization	α_3
4	$e + H_2^+ \rightarrow H^+ + H + e$	Dissociative excitation	α_4
5	$e + H_2 \rightarrow H_2^+ + 2e$	Molecular ionization	α_5
6	$e + H_2^+ \rightarrow H + H^*$	Dissociative recombination	α_6
7	$H_2^+ + H_2 \rightarrow H_3^+ + H$	H_3^+ ion formation	α_7
8	$e + H_3^+ \rightarrow 2H + H^+ + e$	Dissociative excitation	α_8
9	$e + H_3^+ \rightarrow 3H$	Dissociative recombination	α_9
10	$e + H_2 \rightarrow H^+ + H + 2e$	Dissociative ionization	α_{10}
11	$e + H_2^+ \rightarrow 2H^+ + 2e$	Dissociative ionization	α_{11}
12	$e + H_2^+ \rightarrow H^+ + H^* + e$	Dissociative excitation	α_{12}

The input power P_{Penning} is calculated with Eq. (4),

$$P_{\text{Penning}} = \pi e E_\perp^2 / \left(v_\parallel \left| \frac{\partial B}{\partial s} \right| \right) \tag{4}$$

where $\frac{\partial B}{\partial s}$ is the magnetic induction intensity along the magnetic field lines, $E_\perp$ is the electric field perpendicular to the magnetic field lines, and $v_\parallel$ is the electron velocity parallel to the magnetic field lines. Only $E_\perp$ is useful in the Penning ion source.

Generally, plasma species (electrons, ions, and neutrals) transport can be described as [25]

$$\rho \frac{\partial}{\partial t}(w_k) + \rho(\mathbf{u} \cdot \nabla) w_k = \nabla \cdot \mathbf{j}_k + R_k \tag{5}$$

where ρ is the mass density of the working gas, w_k is the mass fraction of the kth species, $\mathbf{u}$ is the flow velocity, $\mathbf{j}_k$ is the flux of k-th species, and R_k is the collision term of the heavy particles derived from the plasma chemical reactions. As with the electrons, the characteristics of ion transport are characteristics of the density of static magnetic flux. The magnetic force is used since it can produce a large ion velocity near the cathode in the azimuthal direction. Ion mobility is also a function of the electric field of ambipolarity. v_k is the ion diffusion velocity.

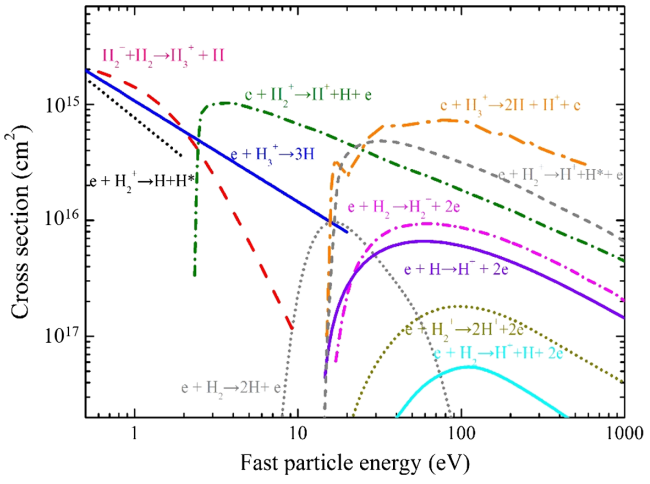

FIG. 6. Cross sections of the main processes of hydrogen plasma inside the ion source [24].

To calculate the fractions of H^+, H^{2+} and H^{3+}, the reactions on the surface are extremely important. The surface reactions of electrons can be expressed as

$$\mathbf{n} \cdot \Gamma_e = \frac{1-r}{1+r}\left(\frac{1}{2} v_{\text{th}} + \mathbf{n} \cdot (\boldsymbol{\mu}_e \cdot \boldsymbol{E})\right) n_e - \left[\sum_i \gamma_i \Gamma_i \cdot \mathbf{n} + \Gamma_t \cdot \mathbf{n}\right] \tag{6}$$

Γ_e is electron flux, Γ_t is thermal electron flux, Γ_i is secondary electron flux. $\mathbf{n} \cdot \Gamma_e$ is the electrons through the surface, $\frac{1-r}{1+r}(\frac{1}{2} v_{\text{th}}) n_e$ is the electrons that disappear or rebound due to the thermal motion in one average-free path, $\sum_i \gamma_i \Gamma_i \cdot \mathbf{n}$ is the secondary electron emission, and $\mathbf{n} \cdot (\boldsymbol{\mu}_e \cdot \boldsymbol{E}) \boldsymbol{n}_e$ is the energy loss of electrons caused by mobility.

The surface reactions of nonelectron species,

$$-n j_k = M_k c_k \mu_k Z_k (nE) + M_k R_{\text{surf},k} \tag{7}$$

where $M_k c_k \mu_k (Z_k n \cdot E)$ represents the drift of nonelectron species and $M_k R_{\text{surf},k}$ represents the thermal motion of nonelectron species. In addition,

$$R_{\text{surf},k} = \sum_i v_{ki}^{\text{f}} q_i, \qquad q_i = k_i^{\text{f}} \prod_k (c_k)^{v_{ki}^{\text{f}}}, \tag{8}$$

where

$$k_i^{\text{f}} = \frac{1}{4} \sqrt{\frac{8RT}{\pi M_n}} (\gamma_i) \prod_{k=\text{surf}} \left(\frac{\sigma_k}{\Gamma_s}\right)^{v_{ki}^{\text{f}}}, \tag{9}$$

γ_i is the dissociative adsorption for certain particles. For H^{3+} and H^{2+}, the most important reaction on the cathodes is the adsorption and recombination reaction

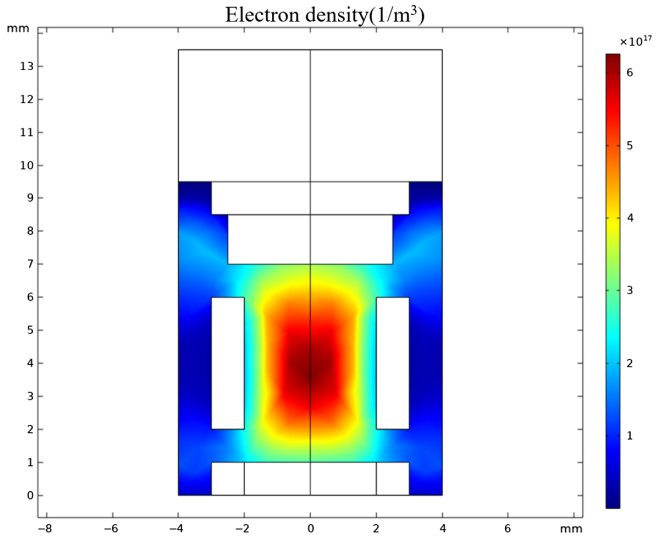

FIG. 7. Plasma simulation results of the Penning source.

$$H + H + \text{cathodes} \rightarrow 2H_2 \tag{10}$$

A simple estimate is based on the plasma cavity size [26]

$$\gamma_{H_2} = \frac{\gamma c}{2R} \tag{11}$$

R is the radius of the cylindrical chamber, γ is the recombination rate, which has a substantial effect on the production of H^+, H^{2+}, and H^{3+} ions at the chamber wall [27].

The coefficient of secondary electron of cathodes with tungsten is assumed as [28]

$$\delta = \frac{3.123 \times (1 + [0.537 - 0.2508 \times \exp(-0.1335W)]}{\cos(\theta)W} \tag{12}$$

where the $W(\text{eV})$ is the energy of the incident electron and θ is the incident angle of the electron.

Based on the plasma model, the plasma of the Penning source is simulated and is shown in Fig. 7. The gas pressure is assumed to be 0.13 Pa (Chap. 6 for details), the anode voltage is set at 1.5 kV based on the experiment, the plasma density simulation result is approximately $5 \times 10^{17}/\text{m}^3$, and the simulation result of the discharge current between the cathode and anode is 0.823 A.

VI. EXPERIMENTAL RESULTS AND OPTIMIZATION

The neutron yield of the neutron tube is positively correlated with the ion energy. Under the same extraction high voltage, the accelerated ion velocity H^+ is greater than $H_2{}^+$, so a higher H^+ fraction is beneficial for neutron yield in neutron tube. A plasma model is proposed to optimize the spacing of the cathodes and increase the proportion of H^+. First, an anode voltage experiment is carried out and compared with the plasma model to verify the reliability of the model and roughly determine the discharge gas pressure in the plasma chamber. In the experiment, we use a needle valve for the hydrogen inlet, and the pressure can only be measured after the extraction system. There is no way to directly measure the pressure in the discharge chamber, so the pressure can only be estimated by the plasma simulation.

Based on the plasma model, the relationship between the anode voltage and current is simulated. When the gas pressure of the plasma model is set at 0.13 Pa, the simulation results and the experiment fit well, as shown in Fig. 8. This also means that when the experimental hydrogen inlet is 0.07 sccm, the pressure inside the source is approximately 0.13 Pa. It is found in the experiment that when the anode voltage exceeds 1650 V at 0.07 sccm, the anode current becomes disordered, and the simulation results stray from the experimental results. This may be because the discharge model has changed; arc discharge occurs when the voltage is too high while the gas pressure is not enough. The arc discharge is a very random discharge, it is difficult to establish a plasma model. Thus, it is not considered in this paper.

Because the size of the discharge chamber of the ion source is too small, it is difficult to use the Langmuir probe to measure the plasma density, and a large number of experimental results also show that the extraction current is not proportional to the plasma density, so the ion ratio will be more reliable to characterize the plasma state in the ion source. Through experiments, it can be found that the gas pressure in the ion source is basically proportional to the flow rate, therefore, the relationship between the gas inlet

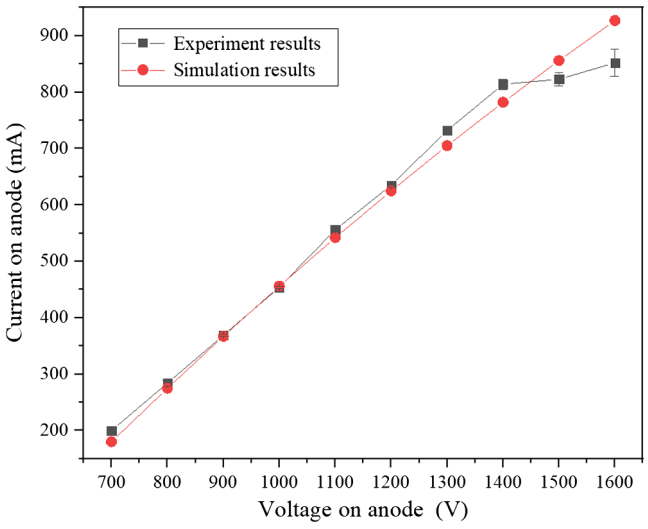

FIG. 8. The experimental and simulation results of the discharge current with respect to the anode voltage (discharge gap fixed at 6 mm).

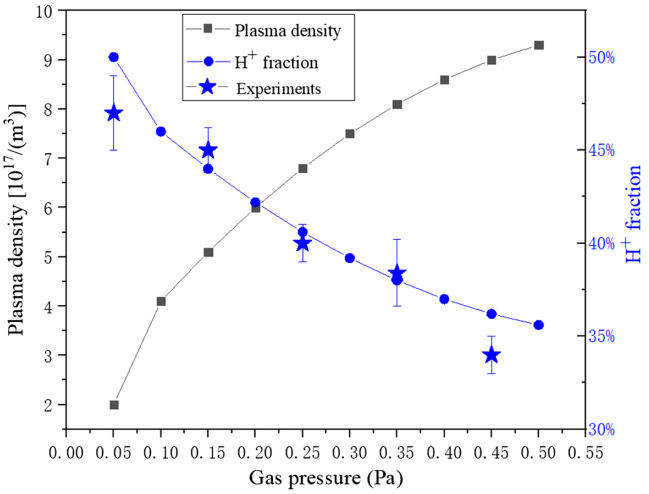

FIG. 9. Simulation and experimental results of plasma density and H^+ fraction at different pressures (anode voltage is fixed at 1.5 kV and discharge gap fixed at 6 mm).

flow and the gas pressure can be obtained through Fig. 8, which is $P(\mathrm{Pa}) = 1.86 \times I_{\mathrm{intake}}(\mathrm{sccm})$. Then the ion ratio measurement of the extracted beam under different gas pressures has been carried out and compared with the plasma simulation results as shown in Fig. 9. It can be seen that as the hydrogen pressure decreases, the H^+ fraction increases, but the total plasma density also decreases. Considering the gas consumption of the neutron tube in the future, the gas pressure is better to not exceed 0.25 Pa, by calculating the total current and H^+ fraction, a value of approximately 0.15 Pa is considered to be the best hydrogen pressure. Based on the experimental hydrogen consumption of 0.08 sccm, the internal pressure of the ion source is estimated to be 0.15 Pa. Of course, for different application scenarios, the discharge conditions can be optimized based on the simulation results.

Since the outer diameter of the Penning source is limited by the neutron tube, the adjustable space for the size of the anode is relatively small, so the optimization simulation and experimental study of the distance between the two cathodes are carried out, as shown in Fig. 10. In the simulation, the anode voltage is fixed at 1.5 kV, and the diameter of the anode is kept at 12 mm. It can be seen in the simulation results that with increasing cathode spacing, the proportion of H^+ gradually increases. The cathode spacing is large enough, and the mean free path of electrons becomes larger. From the hydrogen ionization process in Table II, it can be seen that this leaves more space and time to allow H_3^+ and H_2^+ to be ionized into H^+, resulting in an increased proportion of H^+. However, as the distance between the cathodes increases, the gas in the discharge chamber increases, and when the anode voltage is kept constant, the average power for hydrogen decreases, so the overall plasma density decreases. When the cathode spacing is less than 3.5 mm, the anode becomes very short, and the plasma establishment may not be stable, resulting in a decrease in plasma density. We carried out the experimental comparison of 4, 6, 8, and 10 mm, as shown in the five-point star in Fig. 10. It can be seen from the left panel of Fig. 10 that H^+ fraction simulation results are in good agreement with the experiment. This is a benefit from the correction of the plasma model by the experimental results of the gas pressure ion ratio in Fig. 9. In the right panel of Fig. 10, the extraction current is not in very good agreement with the simulation results, but the overall trend is basically the same. This is because the plasma model cannot include plasma extraction efficiency. For both H^+ fraction and extraction current experiment, when the cathode interval is greater than 6 mm, the stability of the discharge will be deteriorated, which will eventually lead to the difficulty of experiment repeatability and the increase of measurement error. So the value of 6 mm is considered to

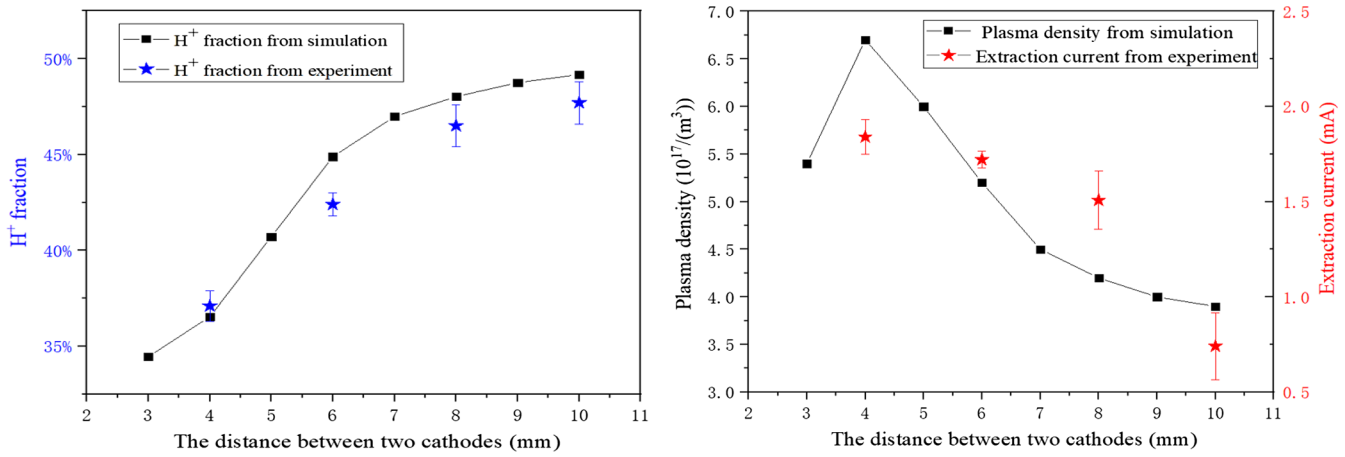

FIG. 10. Plasma simulation and experimental results with different discharge gaps (anode voltage is fixed at 1.5 kV and internal pressure of the ion source is fixed at 0.15 Pa).

be a good cathode spacing, which is able to balance the current intensity and H^+ fraction.

As the distance between the two cathodes changes from the original 4 to 6 mm, and with the optimization of the magnetic field, the beam current is increased from 1.21 mA with 2 kV@1250 mA (2.5 kW), 0.12 sccm hydrogen intake to 1.72 mA with anode power of 1.5 kV × 0.876 A (1.31 kW) and 0.08 sccm hydrogen intake, and the H^+ fraction reaches 42.3%. Although it does not reach the simulated 44.9% fraction, it is still approximately 6% higher than the original 4-mm spacing between the two cathodes. Moreover, with the reduction of the anode power and the gas consumption, the lifetime of the sealed neutron tube with the new Penning source is expected to reach 300 h, which will be a huge improvement for high-flux sealed neutron tubes in oil exploration.

VII. CONCLUSION

A Penning source was developed and tested for the neutron tube. The magnetic field was optimized with soft iron based on the magnetic field and plasma simulations. An extraction system was also optimized, and the diameter of the extraction beam was reduced. A plasma model with Penning discharge via multiphysics simulation was completed using COSMOL 5.5. The experimental and simulation results of the discharge current and H^+ fractions were conducted and compared. The spacing between the two cathodes was optimized based on plasma simulations. By optimizing the magnetic field, extraction system, and cathode spacing, the extraction current of the Penning source reached 1.72 mA, which was 43% higher than the original Penning source current intensity, and the H^+ ratio was increased from 36% to 42.3%. The discharge efficiency and lifetime of the Penning source have been greatly improved.

ACKNOWLEDGMENTS

This work is supported by the National Natural Science Foundation of China Grant No. 12105278, the international partnership program of the Chinese Academy of Sciences Grant No. 211134KYSB20200057 and "the Fundamental Research Funds for the Central Universities". The authors appreciate the help from the USTC Center for Micro and Nanoscale Research and Fabrication and the Hefei Comprehensive National Science Center

[1] Paul Lorrain, A low-pressure glow-discharge proton source, Can. J. Res. **25A**, 338 (1947).

[2] Z. Yang, J. D. Long, P. Dong, T. Wang, T. Wei, X. Z. He, K. Z. Zhang, and J. S. Shi, A preliminary study of a negative hydrogen PIG-type ion source for the compact cyclotron, Chin. Phys. C **36**, 1000–1003 (2012).

[3] J. P. Flemming, Penning source for ion implantation, J. Vac. Sci. Technol. **12**, 1369 (1975).

[4] L. Rovey, B. P. Ruzic, and T. J. Houlahan, Simple Penning ion source for laboratory research and development applications, Rev. Sci. Instrum. **78**, 106101 (2007).

[5] S. Qiao, Q. Fan, Z. Yang *et al.*, Modeling and control of Penning ion source in neutron tube, At. Energy Sci. Technol. **52**, 1316 (2018).

[6] Y. M. Song, H. G. Yang, J. S. Zhang, S. Q. Lu, and T. J. Guo, The parameters test of a sealed D-T logging neutron tube, J. Isotopes **27**, 199 (2014).

[7] P. Arndt, W. Jenter, and H. E. Mahnke, A Penning ion source in a 7-Mv Van De Graaff, IEEE Trans. Nucl. Sci. **22**, 1715 (1975).

[8] B. K. Das and A. Shyam, Development of compact size Penning ion source for compact neutron generator, Rev. Sci. Instrum. **79**, 587 (2008).

[9] D. H. An, I. S. Jung, J. Kang *et al.*, The negative hydrogen Penning ion gauge ion source for KIRAMS-13 cyclotron, Rev. Sci. Instrum. **79**, 1711 (2008).

[10] Z. Nouri, R. Li, R. A. Holt, and S. D. Rosner, A Penning sputter ion source with very low energy spread, Nucl. Instrum. Methods Phys. Res., Sect. A **614**, 174 (2010).

[11] N. V. Mamedov, S. P. Maslennilov, A. A. Solodovnikov, and D. I. Yurkov, Operation features of the pulse penning ion source in the transition pressure range, J. Phys. Conf. Ser. **1393**, 012047 (2019).

[12] D. C Faircloth, A. P. Letchford, C. Gabor, M. O. Whitehead, T. Wood, S. Jolly, J. Pozimski, P. Savage, and M. Woods, Understanding extraction and beam transport in the ISIS H(−) Penning surface plasma ion source, Rev. Sci. Instrum. **79**, 02B717 (2008).

[13] S. K. Sharma, S. Jakhar, R. Shukla, A. Shyam, and C. V. S. Roa, Explosive detection system using pulsed 14-MeV neutron source, Fusion Eng. Des. **85**, 1562 (2010).

[14] J Ghassoun and D. Mostacci, A compact neutron beam generator system designed for prompt gamma nuclear activation analysis, Appl. Radiat. Isot. **69**, 1138 (2011).

[15] https://www.3ds.com/products-services/simulia/products/cst-studio.

[16] A. L. Zhang, S. X. Peng, H. T. Ren, T. Zhang, J. F. Zhang, Y. Xu, Z. Y. Guo, and J. E. Chen, Study on space charge compensation in negative hydrogen ion beam, Rev. Sci. Instrum. **87**, 02B915 (2016).

[17] A. L. Zhang, S. X. Peng, H. T. Ren, T. Zhang, J. F. Zhang, Y. Xu, J. M. Wen, W. B. Wu, Z. Y. Guo, and J. E. Chen, A fast emittance measurement unit for high intensity dc beam, Chin. Phys. B **27**, 025205 (2018).

[18] S. X Peng, A. L. Zhang, W. B. Wu, T. H. Ma, Y. X. Jiang, K. Li, H. T. Ren, T. Zhang, J. F. Zhang, Y. Xu, J. M. Wen, W. B. Wu, Z. Y. Guo, and J. E. Chen, Plasma simulation and optimization for a miniaturized antenna ECR ion source, Nucl. Instrum. Methods Phys. Res., Sect. A **1011**, 165586 (2021).

[19] Q. Luo, A. L. Zhang, and H. P. Peng, Design and simulation of a surface wave-based cylindrical hollow plasma cavity for wakefield booster for future e^+e^- colliders, IEEE Trans. Plasma Sci. **49**, 1848 (2021).

[20] G. J. M. Hagelaar, K. Makasheva, L. Garrigues, and J.-P. Boeuf *et al.*, Modelling of a dipolar microwave plasma sustained by electron cyclotron resonance, J. Phys. D **42**, 194019 (2009).

[21] J. T. Gudmundsson, On the effect of the electron energy distribution on the plasma parameters of an argon discharge: a global (volume-averaged) model study, Plasma Sources Sci. Technol. **10**, 76 (2001).

[22] G. J. M. Hagelaar and L. C. Pitchford, Solving the Boltzmann equation to obtain electron transport coefficients, and rate coefficients for fluid models, Plasma Sources Sci. Technol. **14**, 722 (2005).

[23] W. B Wu, A. L. Zhang, S. X. Peng, T. H. Ma, Y. X. Jiang, K. Li, H. T. Ren, T. Zhang, J. F. Zhang, Y. Xu, J. M. Wen, W. B. Wu, Z. Y. Guo, and J. E. Chen, A global model of 2.45 GHz ECR ion sources for high intensity H^+ H_2^+ and H_3^+ beams, Vacuum 109744 (2020).

[24] R. K. Janev, W. D. Langer, and E. Douglass, Jr., *Elementary Processes in Hydrogen-Helium Plasmas: Cross Sections and Reaction Rate Coefficients* (Springer Science & Business Media, New York, 1987).

[25] A Jüngel and Y J. Peng, A hierarchy of hydrodynamic models for plasmas. Zero-electron-mass limits in the drift-diffusion equations, Ann. Inst. Henri Poincaré, C **17**, 83 (2000).

[26] David Spence and Orville J. Steingraber, Factors determining dissociation fractions in atomic beams generated by "straight-through" microwave discharge sources, Rev. Sci. Instrum. **59**, 2464 (1988).

[27] P. Roychowdhury, L. Mishra, H. Kewalani, and S. Gharat, Hydrogen plasma characterization at low pressure in 2.45 GHz electron cyclotron resonance proton ion source, IEEE Trans. Plasma Sci. **45**, 665 (2017).

[28] Xie Aigen, Chen Yunyun, Wang zusong, and Zhong Kun, Secondary electron emission at incident angle in 0° to 89°, Chin. J. Vac. Sci. Technol. A **35**, 2 (2015).